Molecular signatures of the glass transition in polymers

Tianyi Jin (金天逸),[1] Connor W. Coley,[1,2] and Alfredo Alexander-Katz[3,*]

[1]*Department of Chemical Engineering, Massachusetts Institute of Technology, Cambridge, Massachusetts 02139, USA*
[2]*Department of Electrical Engineering and Computer Science, Massachusetts Institute of Technology, Cambridge, Massachusetts 02139, USA*
[3]*Department of Materials Science and Engineering, Massachusetts Institute of Technology, Cambridge, Massachusetts 02139, USA*

(Received 1 May 2022; accepted 13 July 2022; published 29 July 2022)

The glass transition temperature (T_g) is one of the most fundamental properties of polymers. T_g is predicted by some theories as a sudden change in a "macroscopic" quantity (e.g., compressibility). However, for systems with "soft" glass transitions where the change is gradual it becomes hard to pinpoint precisely the transition temperature as well as the set of molecular changes occurring during this transition. Here, we introduce two new molecular signatures for the glass transition of polymers that exhibit clear changes as one approaches T_g: (i) differential change of the probability distribution of dihedral angles as a function of temperature and (ii) the distribution of fractional of the time spent in the different torsional states. These new signatures provide insights into the glass transition in polymers by directly exhibiting the concept of spatial heterogeneity and dynamical ergodicity breaking in such systems, as well as provide a key step to quantitatively obtain the transition temperature from molecular characteristics of the polymeric systems.

DOI: 10.1103/PhysRevE.106.014506

I. INTRODUCTION

Glasses share similarities with crystalline solids as they are both rigid, but also with liquids as they both have disordered structures [1–3]. For an amorphous polymer, one of the most important and fundamental properties is the glass transition temperature (T_g) that determines the functionality and applications of such materials [4,5]. Traditional computational ways to predict T_g focused on "macroscopic" quantities such as specific volume (or density) [6], potential energy surfaces [7], and free volume [8,9]. These macroscopic quantities show a pseudo-second-order transition around the transition temperature that depends on the quenching rate, while the transition is not necessarily second order or sharp theoretically [10]. However, the glass transition can also be viewed as an "entropy crisis" at the molecular level [11]. Different approaches to find this transition theoretically were proposed from studying spatial heterogeneity, in which the dynamics of parts of systems are different by orders of magnitude [12–19], to replica symmetry breaking [20–23], to the ergodicity breaking point of the distribution function [20,24–28]. At the end, all these theories agree in finding a point at which the system is no longer able to sample all its configurational space within the window of observation.

Along a similar pathway, experimentally, several works applied electron paramagnetic resonance (EPR) spectroscopy to study the relaxation dynamics of glass-forming polymers including PMMA [29–34]. By labeling polymer segments using magnetic probes (with good thermal stability, stiffness, and geometry), and varying the magnetic field at different temperatures, the EPR spectra show distinct shapes around T_g. Furthermore, different dynamic modes of certain types of atoms using the nuclear magnetic resonance (NMR) at T_g [35,36] were observed.

Here we introduce two new measures *in silico*: one directly compares the conformational distributions of the dihedral angles and the other represents the distribution with the fraction of time spent in the trans, gauche− and gauche+ states, to obtain two clear molecular signatures of the glass transition. Our results exhibit a sudden increase in these two signatures associated with a sudden acceleration in the ability of the system to sample new states as the temperature increases. Thus, these two molecular signatures are consistent with generalized reaction coordinates for the glass transition in these systems. We first demonstrate this in a simple two-state model and then apply this measure to different homopolymers.

II. RESULTS AND DISCUSSIONS

A. Sharp and soft glass transition based on macroscopic quantities

We are interested in homopolymers whose mobility is so low that one would consider them as a glass but due to the multitude of relaxation timescales available to these systems, it is not clear how to assign a point to where the glass transition occurs using traditional metrics. In particular, we consider two atactic homopolymers with a common methacrylate backbone: *poly*(methyl methacrylate) (PMMA) and *poly*(2-ethylhexyl methacrylate) (PEHMA) [Fig. 1(a)]. We first run a molecular dynamics (MD) simulations from a fully relaxed state at 650 K and cool the system to 300 K with a constant cooling rate. We use 20 chains with an index of polymerization of 20, which is a typical configuration for MD studies of polymer glass transitions [37]. More

*Corresponding author: aalexand@mit.edu

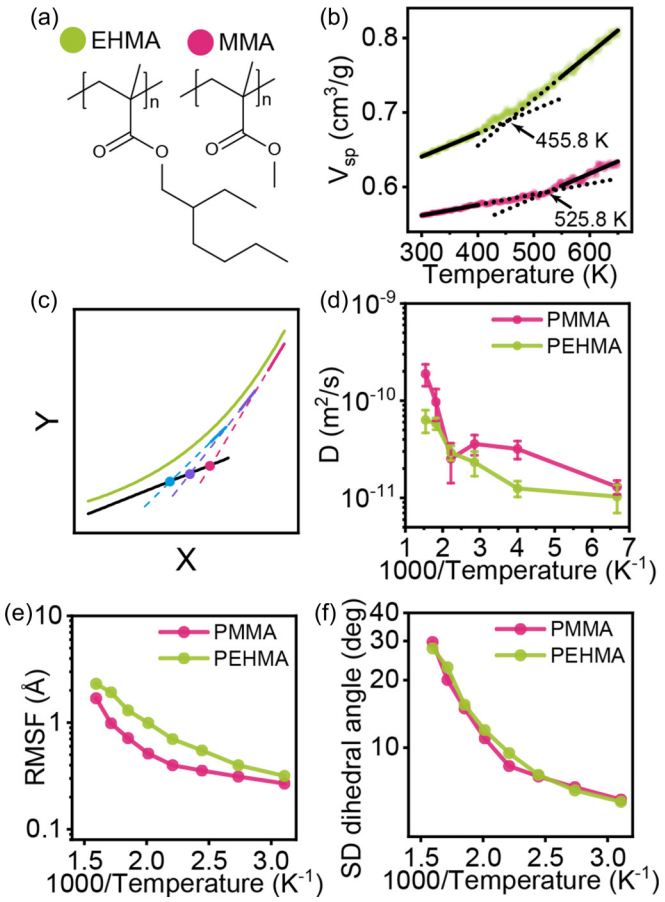

FIG. 1. Glass transition of PEHMA and PMMA from MD simulations using the specific volume (V_{sp}) and mobility measures. (a) Chemical structure of EHMA and MMA and corresponding color codings. (b) Glass transition of PEHMA (soft transition) and PMMA (sharp kink transition) and their corresponding T_g as the intercept of extrapolation (dotted line) from the linear regressions at high and low temperature regime (solid line). (c) Uncertainty of fitting a soft curve using linear extrapolation. (d)–(f) Mobility measures of PEHMA and PMMA: (d) Diffusion coefficient (D), (d) root-mean-square fluctuations of backbone atoms (RMSF) and (f) Standard deviation (SD) of backbone dihedral angle fluctuations. As can be seen, only in the case of PMMA it is possible to pinpoint the transition using V_{sp}, while all the mobility measures do not show a clear transition point and are very similar between both chemistries.

simulation details are provided in the Supplemental Material [40]. The T_g can be predicted based on the slope change of the specific volume (V_{sp}, the inverse of melt density) by using the extrapolated intercept of two linear regressions from high and low temperature regimes [Fig. 1(b)]. As can be seen from the figure, PMMA (red circles) displays a clear kink indicating a glass transition around 525.8 K. Although the experimental T_g values of atactic PMMA are around 400 K [38,39], it is reasonable that our MD simulation overestimates the transition temperature because *in silico* quenching rate is unrealistically higher than the experimental one. While PMMA shows a sharp change in the compressibility, PEHMA shows a smooth decrease in V_{sp} when temperature decreases [note deviations from fitting lines in Fig. 1(c)]. We still categorize PEHMA as a glass because its mobility as characterized by the diffusion coefficient (D), backbone atom fluctuations (RMSF) and backbone dihedral angle fluctuations (SD dihedral angle) is comparable to PMMA, a well-known glass [Figs. 1(d) to 1(f)] (see Sec. C1 of the Supplemental Material for how these quantities are obtained [40]). Here the diffusion coefficient and average dihedral angle fluctuation show inconsistency in the relaxation time; the slopes change at different temperatures. The reason is that, in order for the system to diffuse, large dihedral angle fluctuations are a necessary condition: it is not until most dihedral angles are mobile, when the system can move; but the sufficiency cannot be granted because we only record the backbone dihedral angles. Experimentally, PEHMA behaves as a glass, but does not display any clear change of slope using differential scanning calorimetry (DSC) [41]. Therefore, the appearance of this "soft" glass transition found using MD simulation confirms the experimental results. The qualitative way of explaining the different glass transition behaviors between PMMA and PEHMA is the steric effect of longer side chains preventing the intermolecular movement and leading to a more complex energy landscape, so the T_g of PEHMA is lower and the transition is more smooth. However, the linear extrapolation of PEHMA curve is arbitrary as the slope of the curve continuously decreases: different fitting regimes at high (or low) temperatures (solid line) will result in different intercepts (dot), leading to an artifact when estimating T_g in the soft glass transition [Fig. 1(c)]. Furthermore, within this transition region, such an approach does not contain any information of the changes occurring at the molecular level.

B. Potential energy landscape of glass transition

Glass transitions can be explained by the Potential Energy Landscape (PEL) [42–45] as sketched in a single collective variable (CV) in Fig. 2(a). When a system is supercooled and assuming the crystalline states cannot be formed, it becomes a glass and is trapped in one of the many possible local minima or metastable states. Furthermore, there is a possible existence of an "ideal glass," corresponding to the best and most stable possible glass achievable [46–49]. This ideal glass would have zero configurational entropy, equal to or even lower than that of the crystalline state at the Kauzmann temperature (T_K) [50,51].

When the system is below T_g, almost every part of the system is trapped in a certain local minimum in the observable timescale, however, it is still possible for some parts of the system to escape the glassy state at any finite temperature [red arrow in Fig. 2(a)]. When the system is above T_g, the fraction of the system that can escape the glassy state or rejuvenate will increase dramatically. Therefore, the dynamical heterogeneity of the system will increase in a similar fashion. In other words, if we trace the trajectory of each part of the system (e.g., each backbone dihedral angle), we expect two types of dynamical behaviors: one is locked in one microstate and the other can cross the energy barrier and jump among several microstates. After converting each trajectory during a certain period to the corresponding probability distribution function (PDF) with regard to a generalized coordinate, we will observe a dramatic increase in the *dissimilarity or divergence* among the PDFs

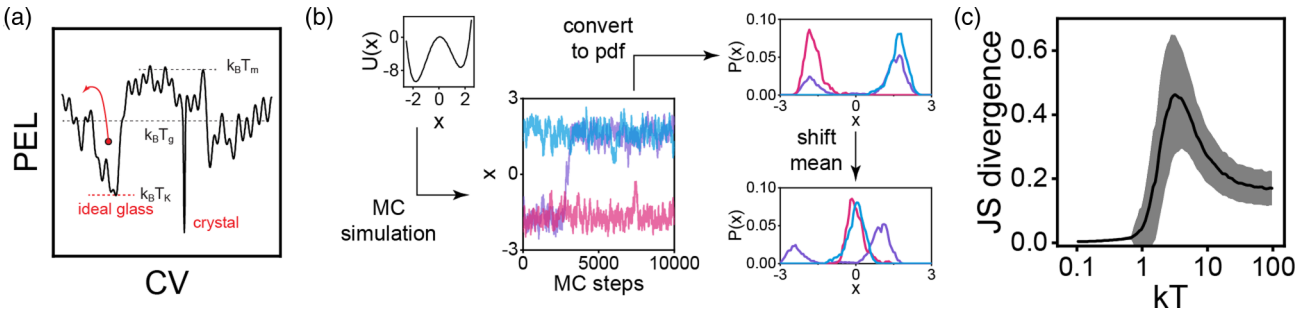

FIG. 2. (a) Schematic representation of a potential energy landscape for a glass former. (b) Energy landscape of a double-well potential and the illustration of calculating the pairwise JS divergence (defined in text) for the double well potentials. The pairwise JS divergence for the distributions shown in (b), left panel are JS (red, blue) = 0.07, JS (red, purple) = 0.99, and JS (blue, purple) = 1.04. (c) The corresponding dynamical heterogeneity (JS divergence) as a function of kT. The error bar is the standard deviation across all pairwise JS divergence.

when the temperature is over T_g. Furthermore, we can expect that at a temperature lower than T_g the dissimilarity among the PDFs is quite low because most parts of the system are locked in a single state. Also, at temperatures much higher than T_g we also expect low dissimilarity since the system can sample all the states (i.e., as an ergodic system) and thus, their PDFs will be similar. Therefore, we expect a maximum in the dissimilarity between PDFs between T_g and the high temperature regime.

C. Simple double-well potential

This behavior can be clearly seen in the simple double-well potential [Fig. 2(b)]. For this system, we run 1000 independent Metropolis Monte Carlo (MC) simulations with random initial positions (see Sec. C2 of the Supplemental Material for the details of the simulations [40]). For these trajectories, we convert them into PDF and shift the mean because if two particles are stuck in two different energy wells, these two PDFs should be classified in the same category (i.e., as a single-state system). Here, we show three independent trajectories in different colors [Fig. 2(b)]. The blue trajectory is stuck in the energy well around $x = 1.7$, the red one is in stuck around $x = -1.7$, and the purple one exhibits a jump between two wells. We convert the trajectories to the corresponding PDFs and then shift the average of the PDFs, so the stuck cases (blue and red) are aligned and show the the highest similarity. We then use the Jensen-Shannon divergence (JS) as the measure of similarity between two discrete distributions $p(x)$ and $q(x)$:

$$\mathrm{JS}(p||q) = \frac{1}{2}\mathrm{KL}(p||M) + \frac{1}{2}\mathrm{KL}(q||M), \tag{1}$$

where M is the average distribution between p and q, i.e., $M(x_i) = \frac{1}{2}[p(x_i) + q(x_i)]$ and KL is the Küllback-Leibler (KL) divergence between two distributions a and b:

$$\mathrm{KL}(a||b) = \sum_i a(x_i)[\log a(x_i) - \log b(x_i)]. \tag{2}$$

Two distributions are identical if and only if JS = 0. See Sec. B of the Supplemental Material for the details of the divergences [40]. The pairwise JS divergence values are as follows: JS (red, blue) = 0.07, JS (red, purple) = 0.99, and JS (blue, purple) = 1.04, suggesting that red and blue are similar to each other but dissimilar to purple. We conduct the Monte Carlo simulations at a kT range from 0.1 to 100 [Fig. 2(c)]. As can be seen from the figure, we see the decreasing trends at both the low and high temperature regions, confirming that the system is dynamically homogeneous in both extreme temperature limits. Furthermore, we also observe a JS maximum in the intermediate temperature at which the system is the most dynamically heterogeneous. Around $kT = 1$, we see a sudden and dramatic increase of system heterogeneity, suggesting the freezing temperature or equivalent T_g coincides with this point, which in this example is around 1. Other features of this molecular signature are that in the low temperature regime, the JS divergence has a nonzero slope related to the increase in the magnitude of fluctuations as a function of kT (Fig. 3). We can see that below the freezing temperature ($kT \approx 1$), the distributions are shrinking from the ten samples at four different temperatures. The mean-shifted PDFs at the same temperature overlap almost exactly. In the high temperature regime for this model, we reach a plateau with a nonzero value for the JS divergence because the system size is effectively growing. It is worth mentioning that the thermal energy (kT) at T_g is lower than both energy barriers $\Delta U = 1.8$ (from $x = -1.7$ to 0.1) and 1.6 (from $x = 1.7$ to 0.1).

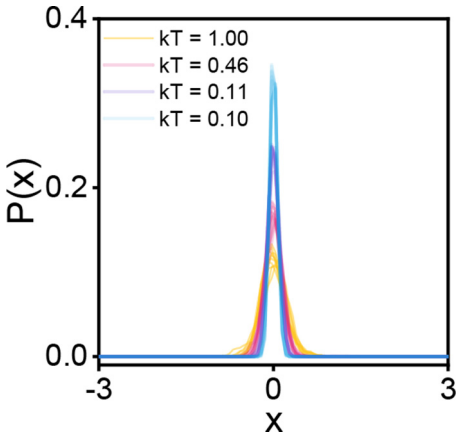

FIG. 3. Probability distribution functions of ten independent trials at four different temperature using Monte Carlo simulation in a double-well potential after mean shift. All temperatures are below the freezing temperature ($kT \approx 1$).

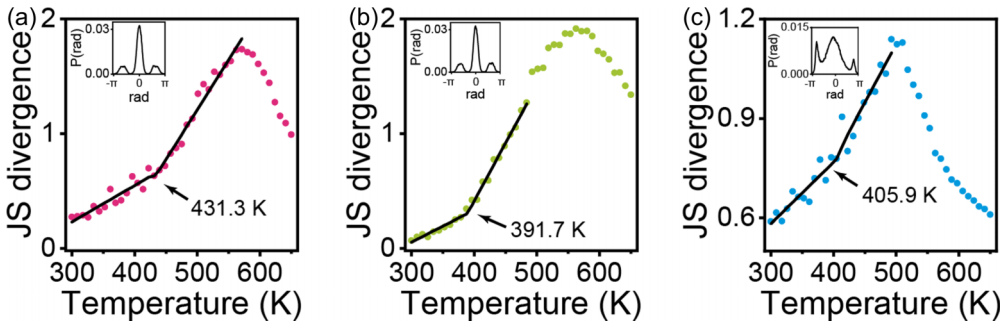

FIG. 4. The dynamical heterogeneity (JS divergence) with regard to temperature for (a) PMMA, (b) PEHMA, and (c) PS. The population probability distribution of backbone dihedral angles is also shown as an inset. The piecewise linear regression is shown as solid line.

D. Homopolymers: Spatial heterogeneity

We then apply the same analysis to both polymeric PMMA and PEHMA systems. Also, we include *poly*(styrene) (PS), a known glassy material as a test of generalizability. Here we run a series of simulations at different temperatures (see Sec. C1 of the Supplemental Material for the details of the simulations [40]). We show the population PDF of dihedral angles as the reference (Fig. 4, insets). This PDF has a globally preferred trans state and favorable gauche− and gauche+ states. The JS divergence among the PDFs of dihedral angles as a function of temperature shows clear signs of a sudden change in dissimilarity between torsional states of different dihedral angles. There is also a maximum between this region and the high temperature regime. We find the sudden change in slope for PMMA and PS at 431.3 K and 405.9 K, respectively (see Table S1 for how smooth or sharp the change in slope is as defined above; see Sec. A of the Supplemental Material for the details of the fits [40]). PEHMA, a glassy material with soft glass transition, however, also shows a sudden increase of slope around 391.7 K. Also, the first segment below the transition temperature has a nonzero slope that also confirms the finding from the double well (Fig. 3). Here we show the average standard deviations among all the dihedral angles below T_g (Fig. 5). The average standard deviations of all systems increase with an increase of temperature.

The T_g values from the new analysis are much more closer to the experimental values compared to V_{sp} from Fig. 1. If we look at the change of V_{sp}, the estimated T_g is comparable to the annealing simulation (Fig. S1). The new analysis also provides a molecular interpretation showing that the glass transition of PEHMA is similar to that of PMMA and PS at the backbone level and that the observed softness in the macroscopic quantities can be due to side chain reconfiguration effects. This suggests that the potential energy landscape of PEHMA is more complex compared to that of PMMA and PS. In other words, there exists a group of identical or at least similar energy barriers in PMMA and PS that determine the glass transition for the backbone, while for PEHMA, there also exists the components from side chains that soften the potential landscape.

E. Homopolymers: Dynamical ergodicity breaking

Finally, we study another relevant definition of the glass transition that is called the dynamical ergodicity breaking. In statistical theory, the term ergodicity refers to where the ensemble average equals the time average, which is a common assumption in equilibrium statistical mechanics. However, for a nonequilibrium system such as glasses, the ensemble average of certain thermodynamic properties can be different from the corresponding time average [52]. Therefore, the point that the ergodicity breaks is the point of the glass transition. Here we proposed a measure to describe the ergodicity of each dihedral angle using the Gaussian mixture model (GMM) (see Sec. D of Supplemental Material for the details of the algorithms [40]).

Previously using JS divergence, we directly compare the distribution functions and find a measure of dynamical heterogeneity. When looking at individual distributions, the shape of the distribution is actually multimodal with each mode representing a specific energy well. If we look at the population distribution function inset in Fig. 4, each function could be decomposed into three different energy wells corresponding to the trans, gauche− and gauche+ states. Therefore, for the individual dihedral angle, we could also decompose its distribution into the three energy wells and measure the fraction of time that it lands in each well. If a dihedral angle is completely locked in one energy well, no matter which one it is in, there will only be one nonzero weight of the modes in the Gaussian mixture model (Figs. S2 and S3). If a dihedral angle is ergodic

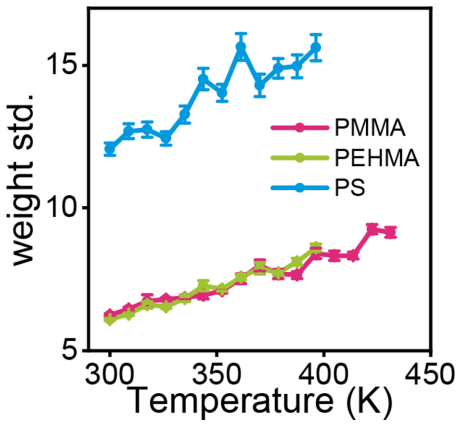

FIG. 5. Average largest standard deviations of all dihedral angles for three homopolymers with increasing temperature. The highest temperature is below the corresponding T_g. The reason for choosing the largest standard deviation is because below T_g, we expect that the majority of dihedral angles are unimodal. The error bar is the standard error across all the dihedral angles.

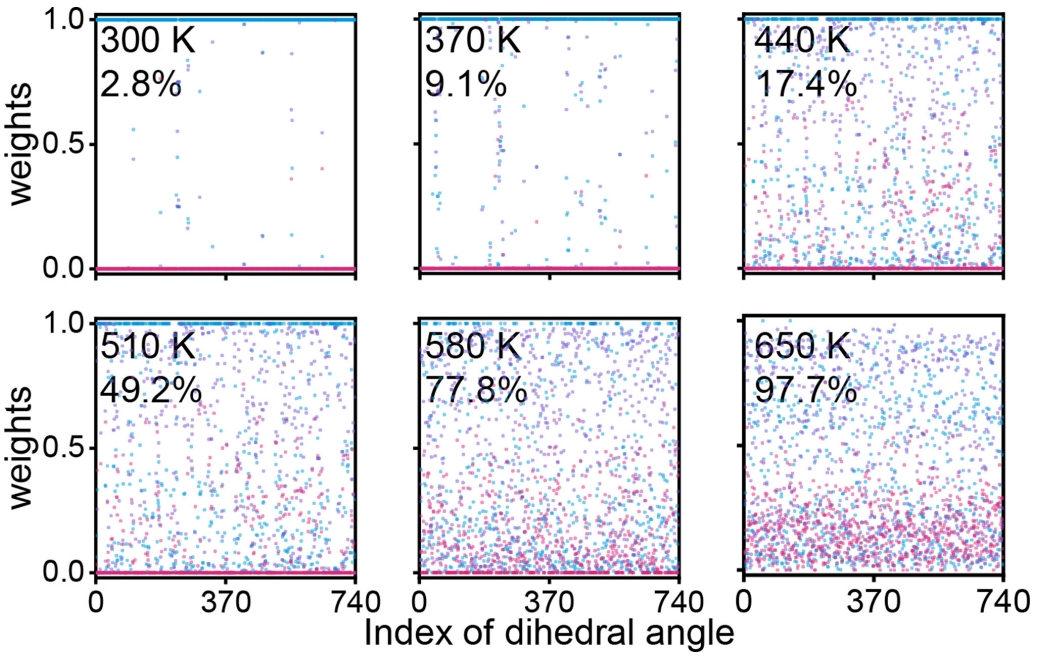

FIG. 6. Sets of weights of individual dihedral angles for MMA at 300 K, 370 K, 440 K, 510 K, 580 K, and 650 K. The three weights in different colors are plotted against the index of all 740 dihedral angles. The percentages of mobile dihedral angles are shown as an inset. A dihedral angles is defined as mobile if the maximum weight is less than 0.95.

or "more" ergodic, from the distribution function, it will exhibit a multimodal PDF and, therefore, more than one nonzero weight. In this sense, we will fit the individual distribution function with a GMM so that the weights, or so-called priors, of each Gaussian will represent the fraction of time spent in each state. Since there are three typical states in these systems (Fig. 4, insets), we fit each distribution with a three-Gaussian model.

The individual weights for all the dihedral angles at different temperature can be found in Fig. 6. We show the sets of weights of each dihedral angle for MMA at six different temperatures (Fig. 6). In each panel, we show the sets for all 740 dihedral angles (x axis). The three weights for each set are in different colors. At 300 K (the left panel in the first row), we can see that most sets have one of the weights equal to unity, meaning that most dihedral angles are completely locked in one energy well (similar cases as the left panel of Fig. S3). Moreover, there are some sets that have more than one nonzero weight (2.8%), representing "ergodic" dihedral angles (similar cases as the middle panel or right panel of Fig. S3). We can see that with the increase of temperature, more dihedral angles became more egordic. At the highest temperature, 650 K, we see that almost all values of weights are nonzero (97.7%), showing that almost all dihedral angles are ergodic.

Then Fig. 7 shows the evolution of three weights ranked and averaged over all the dihedral angles for MMA, EHMA, and PS. We can see that at the low temperature limit, only one out of three weights are close to unity on average indicating the locked states, however, the standard deviations of that weight is nonzero, meaning that there indeed are some dihedrals that are not completely locked and can cross the energy barrier. It is worth mentioning that even at low temperatures (e.g., 300 K), there still exit a small number of mobile and ergodic dihedral angles. This is explained well by the cage effect that even below T_g, there are still mobile part of systems that may be embedded in the frozen parts [53]. We also find there is no clear spatial correlation in the heterogeneity

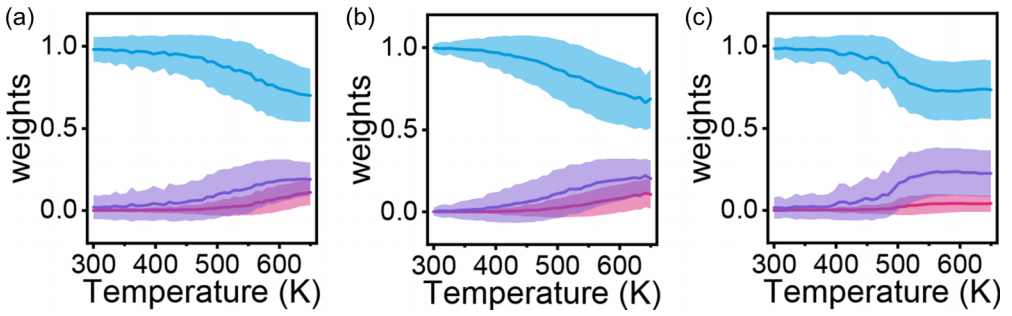

FIG. 7. The fractional occupation of different torsional states with regard to temperature for: (a) PMMA, (b) PEHMA, and (c) PS. For each dihedral angle, the fractions are ranked and then averaged as blue, purple, and red lines. The error bars are the standard deviation across all the dihedral angles. The definition of fractions can be found in Fig. S2 and S3.

(Fig. S4) due to small statistics. Around T_g, there is 17.4% mobile dihedral angles. At the high temperature limit, we see that the weights for PS plateaued, indicating that almost all dihedrals are in their ergodic states. This is corroborated by Fig. 4, which shows that that the JS divergence is similar at the low and high temperature limits, indicating the quantitative heterogeneities are similar: in the low temperature end, almost all dihedrals are locked (with one weight around unity) and in high temperature regime, almost all dihedrals are ergodic (with weights equal to the population). When we look at the shape of the curve, especially the largest weight, we see that for PMMA and PS, there is a sharp increase towards unity as we decrease the temperature. This means that for these two fragile glasses with hard glass transition, the dynamical ergodicity is also sharp and sudden. However, for PEHMA, we see a comparably soft and continuous increase suggesting the ergodicity breaking is also soft (see Table S1 for how smooth or sharp the change in slope is as defined above).

III. CONCLUSION

In summary, we introduce two microscopic signatures to study the glass transition of polymers. The first signature directly compares the configuration distribution functions of backbone dihedral angles using Jensen-Shannon divergence as a measure of system dynamical heterogeneity and the second signature represents each dihedral angle with a set of fractional time spent in the three torsional states. Both of the signatures display a sudden change in their respective quantities at a temperature that we believe is the glass transition. We hypothesize that such a change in the thermodynamic limit would be associated with a kink in the entropy of the system mimicking the behavior of a second order transition. Furthermore, these signatures also provide a way to quantify two major quantities associated with the glass transition: spatial heterogeneity and dynamical ergodicity breaking, at least *in silico*.

As an analogy to the famous mode-coupling theory proposed by Götze [54], these two molecular signatures are independent of the macroscopic quantities such as the compressibility and diffusion coefficient. Instead, based on the sudden increase in the rejuvenated population from the glassy states from the potential energy landscape point of view, we define the transition temperature separately from the macroscopic quantities that are experimentally accessible by using either EPR or NMR. However, this local vibration entropy is less significant in comparison with the configuration entropy (or dihedral angle fluctuation as proposed here) as a contribution to the glass transition [55]. Therefore, this article intends to propose further discussion on this issue.

ACKNOWLEDGMENTS

The authors acknowledge the MIT SuperCloud and Lincoln Laboratory Supercomputing Center for providing computing resources. This work is supported by the Defense Threat Reduction Agency Contract No. HDTRA11910011 and HDTRA12210005.

[1] L. Berthier and G. Biroli, Theoretical perspective on the glass transition and amorphous materials, Rev. Mod. Phys. **83**, 587 (2011).

[2] S. Napolitano, E. Glynos, and N. B. Tito, Glass transition of polymers in bulk, confined geometries, and near interfaces, Rep. Prog. Phys. **80**, 036602 (2017).

[3] F. Arceri, F. P. Landes, L. Berthier, and G. Biroli, Glasses and aging: A statistical mechanics perspective, arXiv:2006.09725.

[4] D. Rigby and R.-J. Roe, Molecular dynamics simulation of polymer liquid and glass. I. glass transition, J. Chem. Phys. **87**, 7285 (1987).

[5] R. J. Young and P. A. Lovell, *Introduction to Polymers* (CRC Press, Boca Raton, FL, 2011).

[6] R. A. Riggleman, H.-N. Lee, M. D. Ediger, and J. J. de Pablo, Free Volume and Finite-Size Effects in a Polymer Glass under Stress, Phys. Rev. Lett. **99**, 215501 (2007).

[7] I. Lyubimov, M. D. Ediger, and J. J. de Pablo, Model vapor-deposited glasses: Growth front and composition effects, J. Chem. Phys. **139**, 144505 (2013).

[8] J. Dudowicz, K. F. Freed, and J. F. Douglas, The glass transition temperature of polymer melts, J. Phys. Chem. B **109**, 21285 (2005).

[9] J. Helfferich, I. Lyubimov, D. Reid, and J. J. de Pablo, Inherent structure energy is a good indicator of molecular mobility in glasses, Soft Matter **12**, 5898 (2016).

[10] A. Zaccone and E. M. Terentjev, Disorder-Assisted Melting and the Glass Transition in Amorphous Solids, Phys. Rev. Lett. **110**, 178002 (2013).

[11] P. G. Wolynes, Entropy crises in glasses and random heteropolymers, J. Res. Natl. Inst. Stand. Technol. **102**, 187 (1997).

[12] J. P. Garrahan and D. Chandler, Geometrical Explanation and Scaling of Dynamical Heterogeneities in Glass Forming Systems, Phys. Rev. Lett. **89**, 035704 (2002).

[13] F. Ritort and P. Sollich, Glassy dynamics of kinetically constrained models, Adv. Phys. **52**, 219 (2003).

[14] L. Berthier and J. P. Garrahan, Real space origin of temperature crossovers in supercooled liquids, Phys. Rev. E **68**, 041201 (2003).

[15] C. Toninelli, G. Biroli, and D. S. Fisher, Spatial Structures and Dynamics of Kinetically Constrained Models of Glasses, Phys. Rev. Lett. **92**, 185504 (2004).

[16] S. Whitelam, L. Berthier, and J. P. Garrahan, Renormalization group study of a kinetically constrained model for strong glasses, Phys. Rev. E **71**, 026128 (2005).

[17] A. C. Pan, J. P. Garrahan, and D. Chandler, Heterogeneity and growing length scales in the dynamics of kinetically constrained lattice gases in two dimensions, Phys. Rev. E **72**, 041106 (2005).

[18] R. L. Jack, P. Mayer, and P. Sollich, Mappings between reaction − diffusion and kinetically constrained systems: A + A ↔ A and the Fredrickson − Andersen model have upper critical dimension $d_c = 2$, J. Stat. Mech.: Theory Exp. (2006) P03006.

[19] M. D. Ediger, Spatially heterogeneous dynamics in supercooled liquids, Annu. Rev. Phys. Chem. **51**, 99 (2000).

[20] A. Heuer, Exploring the potential energy landscape of glass-forming systems: From inherent structures via metabasins to

macroscopic transport, J. Phys.: Condens. Matter **20**, 373101 (2008).
[21] G. Parisi, "Course 6: Glasses, replicas and all that," in *Slow Relaxations and Nonequilibrium Dynamics in Condensed Matter* (Springer, New York, 2003), pp. 271–364.
[22] M. Mézard, G. Parisi, and M. A. Virasoro, *Spin Glass Theory and Beyond: An Introduction to the Replica Method and Its Applications*, Vol. 9, (World Scientific, Singapore, 1987).
[23] T. Castellani and A. Cavagna, Spin-glass theory for pedestrians, J. Stat. Mech.: Theory Exp. (2005) P05012.
[24] L. F. Cugliandolo and J. Kurchan, Analytical Solution of the off-Equilibrium Dynamics of a Long-Range Spin-Glass Model, Phys. Rev. Lett. **71**, 173 (1993).
[25] L. F. Cugliandolo and J. Kurchan, Weak ergodicity breaking in mean-field spin-glass models, Philos. Mag. B **71**, 501 (1995).
[26] A. Barrat, R. Burioni, and M. Mézard, Dynamics within metastable states in a mean-field spin glass, J. Phys. A: Math. Gen. **29**, L81 (1996).
[27] B. Abou, D. Bonn, and J. Meunier, Aging dynamics in a colloidal glass, Phys. Rev. E **64**, 021510 (2001).
[28] M. Schiulaz and M. Müller, Ideal quantum glass transitions: Many-body localization without quenched disorder, in *AIP Conference Proceedings*, Vol. 1610, (American Institute of Physics, College Park, MD, 2014), pp. 11–23.
[29] E. J. Harbron, W. C. Bunyard, and M. D. Forbes, Electron paramagnetic resonance spin probe study of carbon dioxide-induced polymer plasticization, J. Polym. Sci. Part B: Polym. Phys. **43**, 2097 (2005).
[30] Y. Miwa, Novel and accurate method for determination of glass transition temperature of spin-labeled polymer by ESR microwave power saturation, Macromolecules **42**, 6141 (2009).
[31] H. Švajdlenková and J. Bartoš, Spin probe mobility in relation to free volume and relaxation dynamics of glass-formers: A series of spin probes in poly (isobutylene), J. Polym. Sci. Part B: Polym. Phys. **47**, 1058 (2009).
[32] Y. Miwa and K. Yamamoto, Simple and highly sensitive measurement method for detection of glass transition temperatures of polymers: Application of ESR power saturation phenomenon with conventional spin-probe technique, J. Phys. Chem. B **116**, 9277 (2012).
[33] Y. Miwa, T. Kondo, and S. Kutsumizu, Subnanoscopic mapping of glass transition temperature around ionic multiplets in sodium-neutralized poly (ethylene-random-methacrylic acid) ionomer, Macromolecules **46**, 5232 (2013).
[34] F. Zulli, M. Giordano, and L. Andreozzi, Chain-length dependence of relaxation and dynamics in poly (methyl methacrylate) from oligomers to polymers, Macromolecules **51**, 1798 (2018).
[35] S. Sen and J. F. Stebbins, Heterogeneous NO_3^- Ion Dynamics near the Glass Transition in the Fragile Ionic Glass Former $Ca_{0.4}K_{0.6}(NO_3)_{1.4}$: A N^{15} NMR Study, Phys. Rev. Lett. **78**, 3495 (1997).
[36] A. Döß, G. Hinze, G. Diezemann, R. Böhmer, and H. Sillescu, Spatial heterogeneity in glassy polystyrene detected by deuteron NMR relaxation, Acta Polym. **49**, 56 (1998).
[37] J.-L. Barrat, J. Baschnagel, and A. Lyulin, Molecular dynamics simulations of glassy polymers, Soft Matter **6**, 3430 (2010).
[38] J. Biroš, T. Larina, J. Trekoval, and J. Pouchlý, Dependence of the glass transition temperature of poly (methyl methacrylates) on their tacticity, Colloid Polym. Sci. **260**, 27 (1982).
[39] Y. Grohens, M. Brogly, C. Labbe, M.-O. David, and J. Schultz, Glass transition of stereoregular poly (methyl methacrylate) at interfaces, Langmuir **14**, 2929 (1998).
[40] See Supplemental Material at http://link.aps.org/supplemental/10.1103/PhysRevE.106.014506 for which includes Refs. [56–71], for the list of computational details: piecewise linear regression; Küllback-Leibler and Jensen-Shannon divergence; simulation details (molecular dynamics simulation and Monte Carlo simulation) and Gaussian Mixture Model (GMM); And Expectation Maximization (EM) algorithm.
[41] A. Kovalenko, T. Brunet, and O. Mondain-Monval, Mechanical and acoustic properties of macroporous acrylate materials near glass transition, Polymer **148**, 239 (2018).
[42] M. Goldstein, Viscous liquids and the glass transition: A potential energy barrier picture, J. Chem. Phys. **51**, 3728 (1969).
[43] F. H. Stillinger, A topographic view of supercooled liquids and glass formation, Science **267**, 1935 (1995).
[44] P. G. Debenedetti and F. H. Stillinger, Supercooled liquids and the glass transition, Nature (London) **410**, 259 (2001).
[45] F. H. Stillinger and P. G. Debenedetti, Glass transition thermodynamics and kinetics, Annu. Rev. Condens. Matter Phys. **4**, 263 (2013).
[46] S. Singh, M. D. Ediger, and J. J. de Pablo, Ultrastable glasses from in silico vapour deposition, Nat. Mater. **12**, 139 (2013).
[47] C. A. Angell, On the uncertain distinction between fast landscape exploration and second amorphous phase (ideal glass) interpretations of the ultrastable glass phenomenon, J. Non-Cryst. Solids **407**, 246 (2015).
[48] H. Yoon and G. B. McKenna, Testing the paradigm of an ideal glass transition: Dynamics of an ultrastable polymeric glass, Sci. Adv. **4**, eaau5423 (2018).
[49] A. N. Raegen, J. Yin, Q. Zhou, and J. A. Forrest, Ultrastable monodisperse polymer glass formed by physical vapour deposition, Nat. Mater. **19**, 1110 (2020).
[50] W. Kauzmann, The nature of the glassy state and the behavior of liquids at low temperatures., Chem. Rev. **43**, 219 (1948).
[51] F. H. Stillinger, Supercooled liquids, glass transitions, and the kauzmann paradox, J. Chem. Phys. **88**, 7818 (1988).
[52] J. C. Mauro and M. M. Smedskjaer, Statistical mechanics of glass, J. Non-Cryst. Solids **396-397**, 41 (2014).
[53] B. Doliwa and A. Heuer, Cage Effect, Local Anisotropies, and Dynamic Heterogeneities at the Glass Transition: A Computer Study of Hard Spheres, Phys. Rev. Lett. **80**, 4915 (1998).
[54] W. Götze, *Complex Dynamics of Glass-Forming Liquids: A Mode-Coupling Theory*, Vol. 143, (Oxford University Press on Demand, Oxford, 2009).
[55] H. L. Smith, C. W. Li, A. Hoff, G. R. Garrett, D. S. Kim, F. C. Yang, M. S. Lucas, T. Swan-Wood, J. Y. Lin, M. B. Stone *et al.*, Separating the configurational and vibrational entropy contributions in metallic glasses, Nat. Phys. **13**, 900 (2017).
[56] P. Virtanen, R. Gommers, T. E. Oliphant, M. Haberland, T. Reddy, D. Cournapeau, E. Burovski, P. Peterson, W. Weckesser, J. Bright, S. J. van der Walt, M. Brett, J. Wilson, K. J. Millman, N. Mayorov, A. R. J. Nelson, E. Jones, R. Kern, E. Larson, C. J. Carey *et al.*, SciPy 1.0: Fundamental Algorithms for scientific computing in python, Nat. Methods **17**, 261 (2020).
[57] S. Kullback and R. A. Leibler, On information and sufficiency, Ann. Math. Stat. **22**, 79 (1951).

[58] M. Menéndez, J. Pardo, L. Pardo, and M. Pardo, The jensen-shannon divergence, J. Franklin Inst. **334**, 307 (1997).

[59] J. Wang, R. M. Wolf, J. W. Caldwell, P. A. Kollman, and D. A. Case, Development and testing of a general amber force field, J. Comput. Chem. **25**, 1157 (2004).

[60] C. I. Bayly, P. Cieplak, W. Cornell, and P. A. Kollman, A well-behaved electrostatic potential based method using charge restraints for deriving atomic charges: The resp model, J. Phys. Chem. **97**, 10269 (1993).

[61] M. J. Frisch, G. W. Trucks, H. B. Schlegel, G. E. Scuseria, M. A. Robb, J. R. Cheeseman, J. A. Montgomery, Jr. T. Vreven, K. N. Kudin, J. C. Burant, J. M. Millam, S. S. Iyengar, J. Tomasi, V. Barone, B. Mennucci, M. Cossi, G. Scalmani, N. Rega, G. A. Petersson, H. Nakatsuji *et al.*, *GAUSSIAN 03, Revision D.01*, Gaussian, Inc., Wallingford, CT, 2004.

[62] D. Case, I. Ben-Shalom, S. Brozell, D. Cerutti, I. T.E. Cheatham, V. Cruzeiro, T. Darden, R. Duke, D. Ghoreishi, G. Giambasu, T. Giese, M. Gilson, H. Gohlke, A. Goetz, R. H. D. Greene, N. Homeyer, Y. Huang, S. Izadi, A. Kovalenko, R. Krasny *et al.*, *Amber 2019*, University of California, San Francisco, 2019.

[63] R. J. Loncharich, B. R. Brooks, and R. W. Pastor, Langevin dynamics of peptides: The frictional dependence of isomerization rates of n-acetylalanyl-n′-methylamide, Biopolymers: Original Research on Biomolecules **32**, 523 (1992).

[64] J.-P. Ryckaert, G. Ciccotti, and H. J. Berendsen, Numerical integration of the cartesian equations of motion of a system with constraints: Molecular dynamics of n-alkanes, J. Comput. Phys. **23**, 327 (1977).

[65] H. J. Berendsen, J. V. Postma, W. F. van Gunsteren, A. DiNola, and J. R. Haak, Molecular dynamics with coupling to an external bath, J. Chem. Phys. **81**, 3684 (1984).

[66] U. Essmann, L. Perera, M. L. Berkowitz, T. Darden, H. Lee, and L. G. Pedersen, A smooth particle mesh ewald method, J. Chem. Phys. **103**, 8577 (1995).

[67] L. Martínez, R. Andrade, E. G. Birgin, and J. M. Martínez, Packmol: A package for building initial configurations for molecular dynamics simulations, J. Comput. Chem. **30**, 2157 (2009).

[68] A. Einstein, Über die von der molekularkinetischen theorie der wärme geforderte bewegung von in ruhenden flüssigkeiten suspendierten teilchen, Ann. Phys. (Leipzig) **322**, 549 (1905).

[69] M. von Smoluchowski, Zur kinetischen theorie der brownschen molekularbewegung und der suspensionen, Ann. Phys. (Leipzig) **326**, 756 (1906).

[70] S. van der Walt, S. C. Colbert, and G. Varoquaux, The numpy array: A structure for efficient numerical computation, Comput. Sci. Eng. **13**, 22 (2011).

[71] D. R. Roe and T. E. Cheatham III, Ptraj and cpptraj: Software for processing and analysis of molecular dynamics trajectory data, J. Chem. Theory Comput. **9**, 3084 (2013).